Adv. Polar Upper Atmos. Res., 16, 59–83, 2002

Comparison of flow angle variations of E-region echo characteristics at VHF and HF

R.A. Makarevitch[1], A.V. Koustov[1], K. Igarashi[2], K. Ohtaka[2], T. Ogawa[3], N. Nishitani[3], N. Sato[4], H. Yamagishi[4] and A.S. Yukimatu[4]

[1]*Institute of Space and Atmospheric Studies, University of Saskatchewan, 116 Science Place, Saskatoon, S7N 5E2 Canada*
[2]*Communications Research Laboratory, Tokyo 184-8795*
[3]*Solar-Terrestrial Environment Laboratory, Nagoya University, Honohara, Toyokawa 442-8507*
[4]*National Institute of Polar Research, Kaga 1-chome, Itabashi-ku, Tokyo 173-8515*

Abstract: In this study, characteristics of the auroral E-region echoes at two significantly different radar frequencies of 12 and 50 MHz are compared. Considered observations were performed at the Syowa Antarctic station in March of 1997 using two HF and one VHF radars at various angles with respect to the magnetic L shells. The diurnal variation of echo occurrence was found to be similar at two frequencies and consistent with previous studies. On the other hand, variation of echo occurrence with L-shell angle ϕ was shown to be significantly different at two frequencies. 50-MHz echoes were detected preferentially along the L shell (dominating direction of the electrojet flow) while 12-MHz echoes were detected in a broad range of azimuths with the maximum in echo occurrence at $\phi \cong 40$–$50°$. By plotting the Doppler velocity versus L-shell angle, we demonstrate that 12-MHz echoes can be divided into two populations, the high- and low-velocity echoes. The high-velocity echoes were observed mostly along the L shells while the low-velocity echoes were observed at all directions. We also show that the echo populations exhibit different variation of the Doppler velocity with the L-shell angle. We argue that while the 50-MHz echoes are related to the Farley-Buneman and gradient drift plasma instabilities, the 12-MHz echoes can have additional sources, such as the thermo-diffusion instability and/or neutral wind-related plasma instabilities.

1. Introduction

Meter-scale auroral E-region irregularities have been traditionally studied with VHF coherent radars (see review papers by Fejer and Kelley, 1980; Haldoupis, 1989; Schlegel, 1996; Sahr and Fejer, 1996). Recent deployment of the Super Dual Auroral Radar Network (SuperDARN or SD) system of coherent HF radars has provided opportunities for studies of ionospheric irregularities in the decameter band (Villain *et al.*, 1987, 1990; Milan and Lester, 1998, 1999, 2001; Milan *et al.*, 2001; Fukumoto *et al.*, 1999, 2000; Jayachandran *et al.*, 2000; Koustov *et al.*, 2001; Makarevitch *et al.*, 2001; Uspensky *et al.*, 2001; Ogawa *et al.*, 2001).

It has been shown that the characteristics of HF echoes are often quite different from

the ones established at VHF. Milan and Lester (1999) were the first who described several new types of HF echoes, in addition to classical type 1 and type 2 echoes that are traditionally related to the Farley-Buneman (F-B) and gradient drift (G-D) plasma instabilities. These authors considered data of the SD Iceland East radar observing predominantly along the direction of the magnetic L shells. Jayachandran *et al.* (2000), after studying Saskatoon SD radar data at large L-shell angles, proposed to consider separately a new class of HF echoes which they termed "the slow long-lived E-region plasma structures (SLERPs)". SLERPS are very stable, spatially and temporally, echoes with low velocities. Jayachandran *et al.* (2000) attributed SLERPS' generation to the G-D plasma instability. Ogawa *et al.* (2001) reported on short-range low-velocity HF echoes observed at the Syowa Antarctic station that were related to the effects of neutral wind and neutral turbulence.

New information on the issue has been given in recent studies by Koustov *et al.* (2001) and Makarevitch *et al.* (2001). These authors considered Syowa SD measurements that were supplemented by nearly simultaneous VHF measurements. Analysis of the velocity relationship at HF and VHF showed that the HF echoes could be divided into two categories, the high- and low-velocity echoes. The high-velocity echoes were observed mostly along the L shells while the low-velocity echoes were observed at all directions. The high-velocity echoes were related to the F-B plasma instability while the nature of the low-velocity echoes was not discussed.

Nearly simultaneous VHF and HF coherent observations of E-region echoes are of special interest since they provide information on irregularity characteristics at two quite different scales. Such measurements become even more important if the plasma instabilities that are responsible for the irregularity formation are the same for the two scales. In the previous studies by Koustov *et al.* (2001) and Makarevitch *et al.* (2001) data on the echo power and Doppler velocity were discussed. In this paper we expand the above studies by considering much larger data sets and also by considering other echo characteristics such as occurrence rate and HF spectral width. Our main focus is on properties of E-region HF and VHF echoes as a function of the direction of observations.

2. Observations

We use measurements from two SENSU HF SuperDARN radars (Syowa East and Syowa South, ~12 and ~11 MHz, respectively) operated by the National Institute of Polar Research and one VHF coherent radar (~50 MHz) run by the Communications Research Laboratory (CRL). All three radars are located at Syowa (69.0°S, 39.6°E, magnetic latitude ~67°). Figure 1 shows the experimental setup with the near (slant ranges r less than 900 km) field of view (FoV) of the Syowa East (blue sector) and Syowa South (green sector) radars. FoV of the CRL radar for $r<1000$ km is shown by the yellow sector. The solid red curve represents the line of zero off-perpendicular (aspect) angle ($\alpha=0$) at 110-km altitude, assuming no refraction for radio waves, and the circular dashed white lines are the slant range marks ($r=400$, 600, and 800 km). The thick black lines in Fig. 1 are the Polar Anglo-American Coordinate System (PACE) magnetic parallels or L shells (Baker and Wing, 1989).

In this study we formulate results in terms of L-shell angle ϕ defined as the angle between the direction of the radar wave vector $\mathbf{k}$ and the magnetic L shell. The L-shell

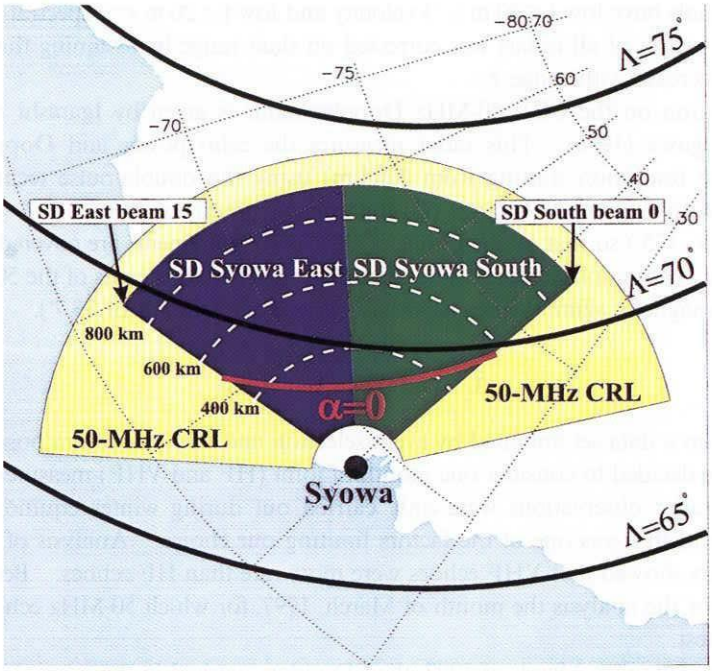

Fig. 1. Near field of view of the Syowa East (blue sector) and Syowa South (green sector) SuperDARN (Super Dual Auroral Radar Network) HF radars. The yellow sector corresponds to the field of view of the Communications Research Laboratory VHF radar. Also shown are PACE (Polar Anglo-American Experiment) lines of equal magnetic latitudes $\Lambda=65°$, $\Lambda=70°$, and $\Lambda=75°$. Thick red curve is the zero off-orthogonal (aspect) angle line ($\alpha=0°$). The white dashed circular lines are range marks of 400, 600, and 800 km.

angle within Syowa East and Syowa South FoVs is positive and changes continuously from $\phi\cong 20°$ (eastern edge of HF FoV, Syowa East beam 15, Fig. 1) to $\phi\cong 140°$ (western edge of HF FoV, Syowa South beam 0). The azimuth corresponding to the L-shell angle of 90° is located close to the eastern edge of the Syowa South FoV, and we will call the radar directions close to this azimuth "perpendicular directions" or "directions perpendicular to the flow". The radar directions close to the edges of the common FoV (Syowa East beam 15 and Syowa South beam 0) will be called "parallel directions" or "directions along the flow", even though the L-shell angle is not exactly zero or 180°. In this terminology we assume that the flow is predominantly along the L shells.

The Syowa HF radars are analogous to all other SD radars in the network (Greenwald *et al.*, 1995). Each radar scans through 16 successive beam positions in 3.33° steps, covering a ~53° range of azimuths. One full scan in a normal mode lasts 2 min, so that every 2 min there are data on the spectral power, mean Doppler shift, and spectral width of echoes in each of 75 range cells (starting from a range of 180 km with a 45-km step) in which scattered signal is detected. No interferometer measurements of an angle of echo arrival (or echo height) were available for Syowa. During HF data postprocessing, ground-scattered signals were removed from the records by applying the standard criteria

that such signals have low (<50 m s^{-1}) velocity and low (<20 m s^{-1}) spectral width. For the analysis, power of all radars was corrected on slant range by assuming that there is an r^{-3} power decrease with range r.

Information on the CRL 50-MHz Doppler radar is given by Igarashi *et al.* (1995, 1998) and Ogawa (1996). This radar measures the echo power and Doppler velocity (15-km range resolution starting from 120 km) using the double-pulse technique. The radar scans with a 5° step in a range of geographic azimuths of 48.7°- 218.7° (geomagnetic azimuths of 5°-175°) so that all directions of the SD measurements are covered. One scan through FoV is accomplished in 4 min. Below we refer to the beams of the 50-MHz radar by their geomagnetic azimuth (beam 40 has geographic azimuth of 83.7°).

3. Database selection

To obtain a data set unbiased by event selection and with maximum possible number of records we decided to consider one month of joint (HF and VHF) measurements. The CRL VHF radar observations were only carried out during winter/equinox seasons of 1995-1997, and this was one of the factors limiting our choice. Analysis of the HF and VHF data sets showed that VHF echoes were more rare than HF echoes. Because of that we selected for the analysis the month of March, 1997, for which 50-MHz echo occurrence was the highest.

Among 31 days in March of 1997, the SD radars worked in the normal (as described in the previous section) mode of operation only during 23 days, and we selected these days. To exclude possible F-region echoes we restricted the slant ranges of all radars by 810 km. And, finally, HF echoes with unusually large spectral width (>500 m s^{-1}) and HF and VHF echoes with low uncorrected power (<3 dB at HF and <1 dB at VHF) were excluded from the database.

4. Diurnal variation of echo occurrence

We first assess the echo occurrence for all three systems during the selected period. Figure 2 shows the total number of echoes as a function of the universal time at 12 MHz (upper panel) and 50 MHz (bottom panel). Here we marked data obtained by Syowa East and Syowa South as 12 MHz though the radars used slightly different frequencies (we will neglect by this difference below for simplicity of presentation).

The number of echoes in Fig. 2 was computed as follows. Since the FoV of the VHF radar is broader than the combined FoVs of the two HF radars, we considered only those VHF radar directions that were within this combined HF FoV. Then, we computed the total number of echoes for all directions and for all near slant ranges ($r<810$ km for all radars) for each 30-min period of time. The universal time is approximately equal to the magnetic local time (MLT) for the near FoV of the Syowa radars (UT$\cong$MLT), therefore Fig. 2 essentially presents the number of echoes for both frequencies as a function of MLT. For comparison we provide the results from Hanuise *et al.* (1991) for the radar frequency of 12 MHz (open circles) and data from Saskatoon IGY auroral radar (McNamara, 1972) at 50 MHz (diamonds) in arbitrary scale. For these radars the universal time differs significantly from the magnetic local time so that we shifted their data to account for this

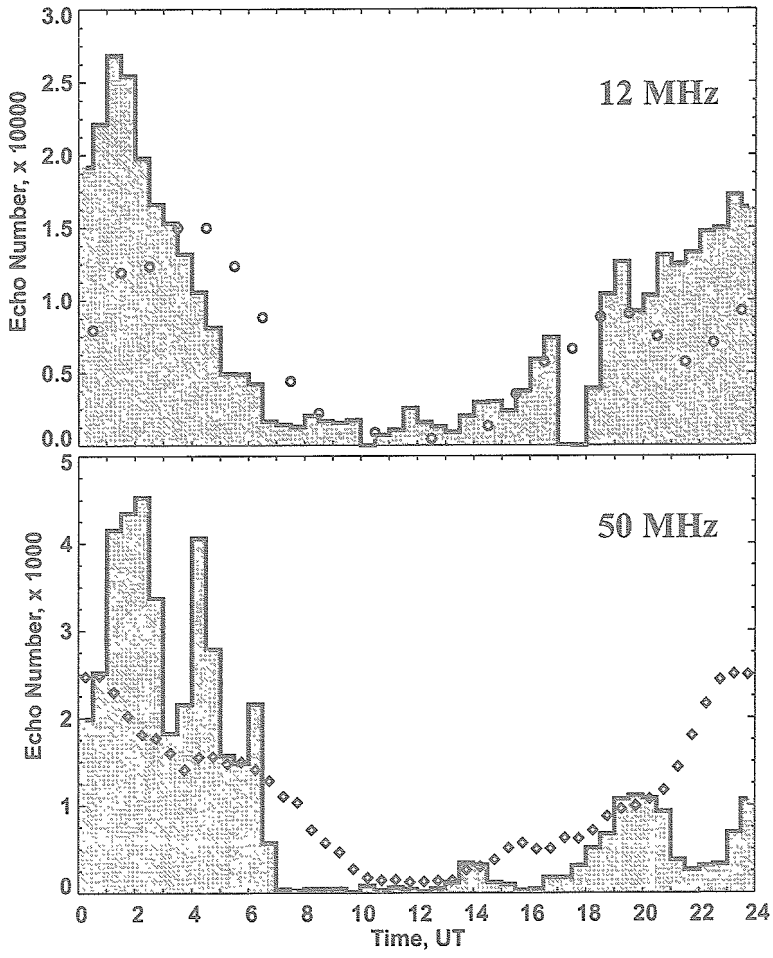

Fig. 2. Number of echoes in the near field of view detected in all available beams as a function of universal time at 12 MHz (upper panel) and 50 MHz (bottom panel). The open circles in the upper panel represent data of Hanuise et al. (1991) for their HF observations (the scale is arbitrary), and the diamonds in the bottom panel show number of 50-MHz echoes versus time from McNamara (1972).

difference.

One can see that the number of echoes at 12 MHz exhibits a clear maximum around 0100 UT and that there are significantly fewer echoes during the daytime (7-19 UT). This result is in reasonable agreement with the data of Hanuise *et al.* (1991), except of slight shift in the location of the maxima (~5 MLT *vs* ~1 MLT).

The similar maximum can be seen at 50 MHz (bottom panel of Fig. 2). The maximum is broader here (1-4 UT), the number of echoes during the evening (18-24 UT) is much less than that at 12 MHz, and there are almost no echoes between 7 and 17 UT. The data of McNamara (1972) show smoother variation with time and the maximum is shifted (~0 MLT *vs* ours ~3 MLT), but, overall, the shape of the curve is similar.

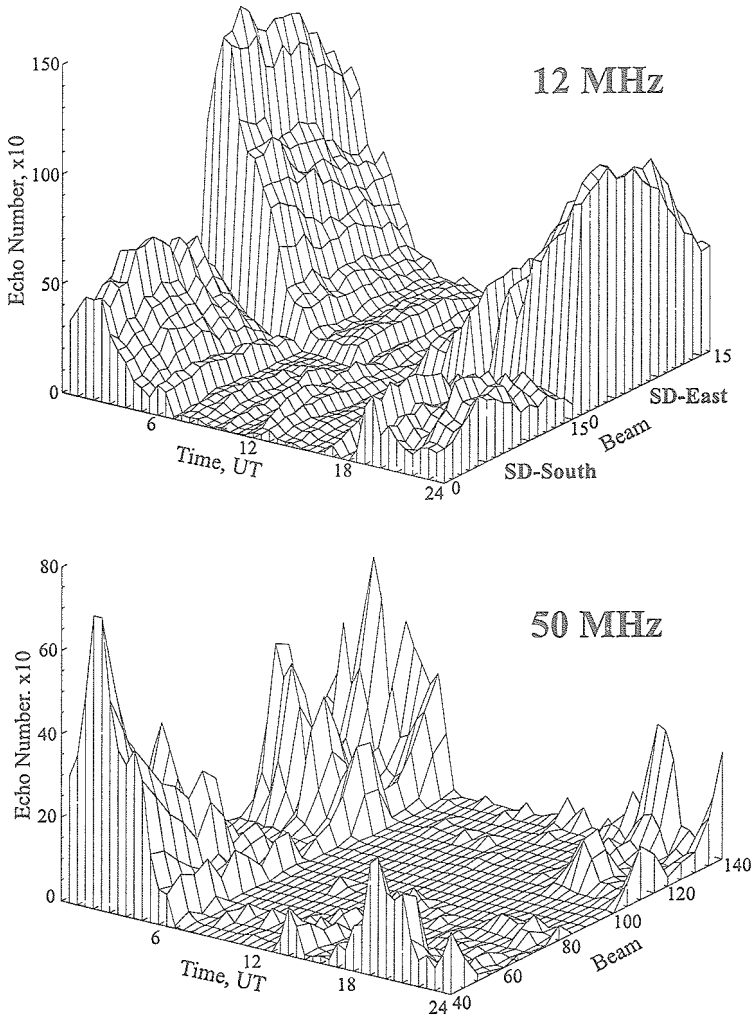

Fig. 3. Variation of number of echoes in the near field of view with radar beam number and universal time at 12 MHz (upper panel) and 50 MHz (bottom panel).

The absence of echoes during some specific times (1000–1030 UT and 1700–1800 UT in the upper panel) at HF is due to the fact that HF radars simply were not operational during these periods. The reasons for the existence of the local minima at VHF (0300–0400 and 0500–0600 UT in the bottom panel) are not clear. We believe that this is most likely because of the smaller data set at VHF (the number of echoes at HF is several times larger than that at VHF).

Figure 2 gives the overall occurrence in the common FoV. In Fig. 3 we present more detailed information. Here we plotted the number of echoes as a function of the time of the day and radar direction, see surfaces for 12 and 50 MHz (upper and bottom panels, respectively). Notice that the number of echoes for Syowa East is 2– 3 times larger than that for Syowa South. However, there is no significant difference between various beams

for individual radars; the azimuthal distribution of echoes is more or less homogeneous for each HF radar. One can notice that for every UT sector the number of echoes is only slightly larger for central beams of each HF radar.

At 50 MHz the situation is completely different. The number of echoes varies with azimuth of observations/beam number. There are almost no echoes detected for 50-MHz beams 80–100 and the number of echoes is at maximum at the edges of common FoV (50-MHz beams 40 and 140).

5. Echo occurrence within FoV

Our next step is to include into analysis slant range information. We consider here echo occurrence versus range and azimuth for the morning observations between 02 and 06 UT when the echo occurrence is at maximum for both HF and VHF (see previous section). We also expect that for this interval the plasma flow is mostly L-shell aligned.

Figure 4 is a contour plot of number of echoes (azimuth of observations horizontally, slant range vertically) for the near FoVs (180–765 km) of 12-MHz (upper panel) and 50-MHz (bottom panel) radars. The red curve on these plots is the line of perfect aspect angle ($\alpha=0$) at the height of 110 km, calculated for each radar by assuming the ionospheric electron density profile from the International Reference Ionosphere-95 (IRI-95) model (Bilitza, 1997). Dashed yellow lines in Fig. 4 are contours of equal L-shell angle ϕ (contour steps are 20°), computed using the PACE magnetic field model. Data from both SD radars were combined in the upper panel of Fig. 4; the transition between two adjacent SD FoVs occurs at an azimuth of ~135°, where the echo occurrence contours change drastically. The FoV of the 50-MHz radar is about 170°-wide; we show 50-MHz data for only those directions that are close to the SD radar directions.

In the 12-MHz part of the diagram one can recognize two distinct areas: close slant ranges (200–500 km), where the distribution of echo occurrence is almost homogeneous with azimuth (except for the noticed earlier difference in number of echoes between two SD radars) and farther ranges (500–765 km) where echoes tend to occur close to the perpendicular directions. There is a clear gap between echoes at closer and farther ranges. For the perpendicular directions, the gap is located at ~480 km and it is quite narrow while for the edges of HF FoV (azimuths of 82° and 184°) it is much wider (there are no echoes detected for $r=500$–765 km). The location of the radar cells with maximum number of echoes follows closely the perfect aspect line, except for the fact that they are shifted slightly to closer ranges. The shift seems to increase towards the edges of the FoV. Interestingly, for the eastern sector (Syowa East) there is a broad global maximum ($\phi=40$–60°, azimuth=95–115°) with some local peaks (orange spots). For the southern sector the maximum is smaller (500 echoes *vs* 1000) and its azimuthal location is $\phi=100$–120°, azimuth=150–170°. Thus the maxima of echo occurrence are somewhere between the parallel and perpendicular directions. In our opinion, echoes from the nearest ranges ($r<500$ km) are originated from the E-region heights (aspect angles at the electrojet heights of 110 km are around zero for this area) while echoes from farther ranges are most probably originated from the bottom/central part of the F region. The far range echoes can also be obtained through the one and half hop propagation mode for which radar waves are refracted in the lower ionosphere and then reflected by the ground towards irregularities.

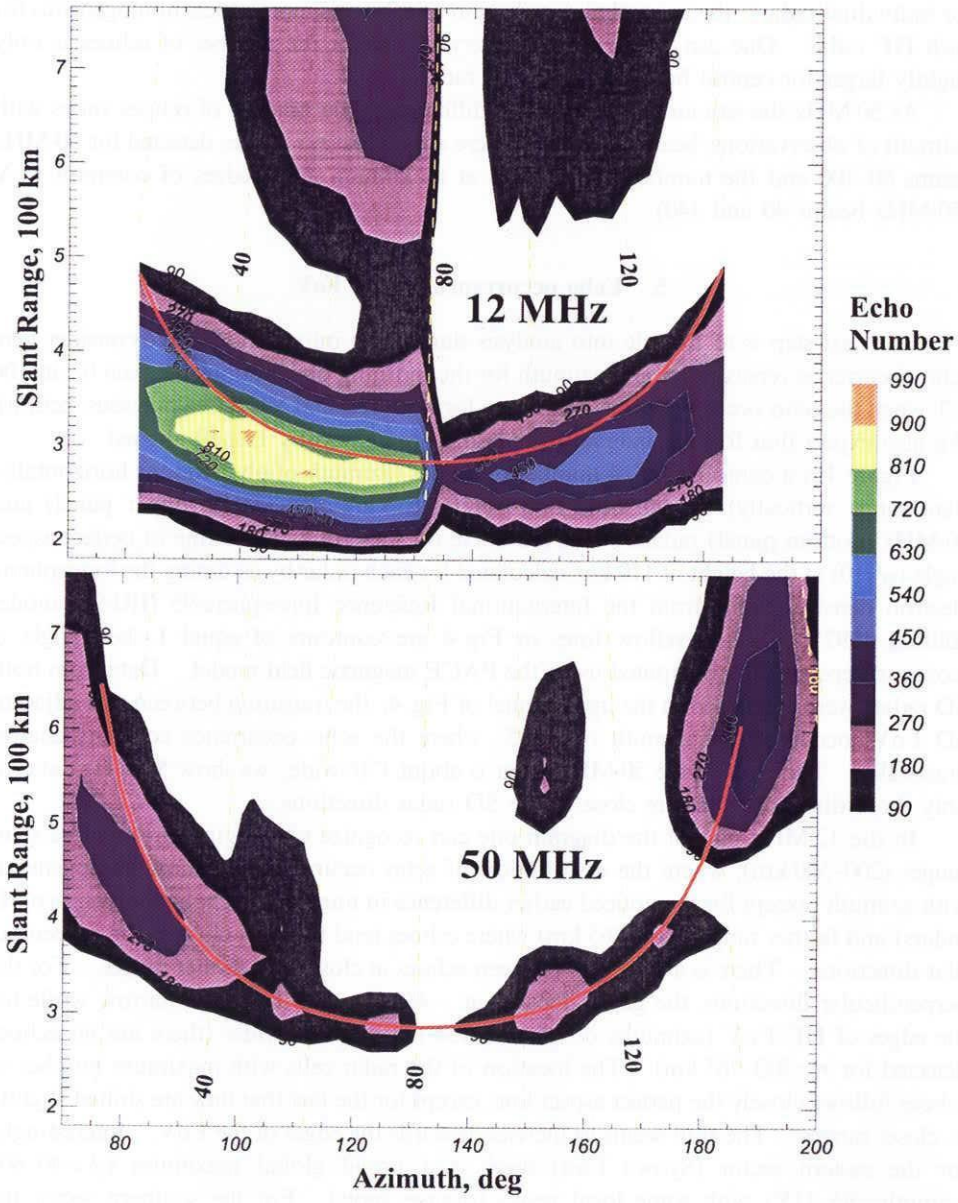

Fig. 4. Number of echoes for various azimuths of observations (horizontal) and slant ranges (vertical) for 12- (upper panel) and 50-MHz (bottom panel) radars. Red solid curves are the zero aspect angle lines calculated by assuming the International Reference Ionosphere-95 (IRI-95) electron density distribution. Dashed yellow lines are the contours of equal L-shell angle (the step is 20°) calculated by assuming the Polar Anglo-American Conjugate Experiment (PACE) magnetic field model.

At 50 MHz (bottom panel) the echo occurrence distribution is quite different (in agreement with Fig. 3). There are no echoes for slant ranges greater than 650 km for perpendicular directions and the shift between the perfect aspect angle line and the location (in slant range) of maxima in echo occurrence is smaller than that at 12 MHz, especially for the perpendicular directions. But the most striking feature in the 50-MHz diagram is that distribution of echo occurrence with azimuth is not homogeneous as at 12 MHz. The number of echoes increases with departure from the perpendicular directions. It maximizes at L-shell angles of 20° and 150° for the eastern and southern sectors of the VHF radar FoV, respectively.

6. Average echo power within FoV

Occurrence diagram of Fig. 4 reflects only the fact of echo presence, and does not tell us how strong was the echo. We address this issue in this section.

In Fig. 5 we show average power in a format similar to Fig. 4. To produce this diagram, we averaged the range-corrected power and plotted it as a function of azimuth and slant range. Similar to the echo occurrence diagram, here and in the next section we consider only observations between 02–06 UT to limit ourselves to the period of maximum in echo occurrence.

One can see that distribution of 12-MHz power is essentially the same as distribution of number of echoes. One can see the stripe of E-region echoes at short ranges and F-region echoes at farther ranges. Within the stripe of E-region echoes, power decreases gradually by ~2–4 dB from maximum at the edges to the center of FoV. The difference between average power for the Syowa East and the Syowa South radars is ~6 dB.

At 50 MHz, there is quite substantial variation of power with azimuth; the difference in power between parallel and perpendicular directions is ~10 dB and power maximizes at L-shell angles of ~20° and ~150°. We will consider data on spectral power for both HF and VHF in more detail later.

7. Average velocity within FoV

Our next step is to consider variations of the Doppler velocity with range and azimuth, Fig. 6. One can see that along the stripe of E-region echoes, the velocity changes from -400 m s^{-1} at the eastern edge of the HF radar FoV to $+300$ m s^{-1} on the western edge. Similar velocities were measured by the VHF radar. The change of the velocity polarity occurs at the azimuth of ~130–140°, close to the perpendicular directions. Obtained average velocities along and perpendicular to the L shells are consistent with much larger data set considered by Ogawa *et al.* (2001).

The HF radars measurements show larger velocities at farther ranges, above the line $\alpha=0$. These measurements are very likely affected by the F-region contributions (Makarevitch *et al.*, 2001; Ogawa *et al.*, 2001). The VHF radar echoes also have large average velocities at far ranges (650–765 km) and azimuths of ~180°. We think, however, that these measurements do not necessarily reflect the general tendencies since the number of echoes for these areas is very low (Fig. 4).

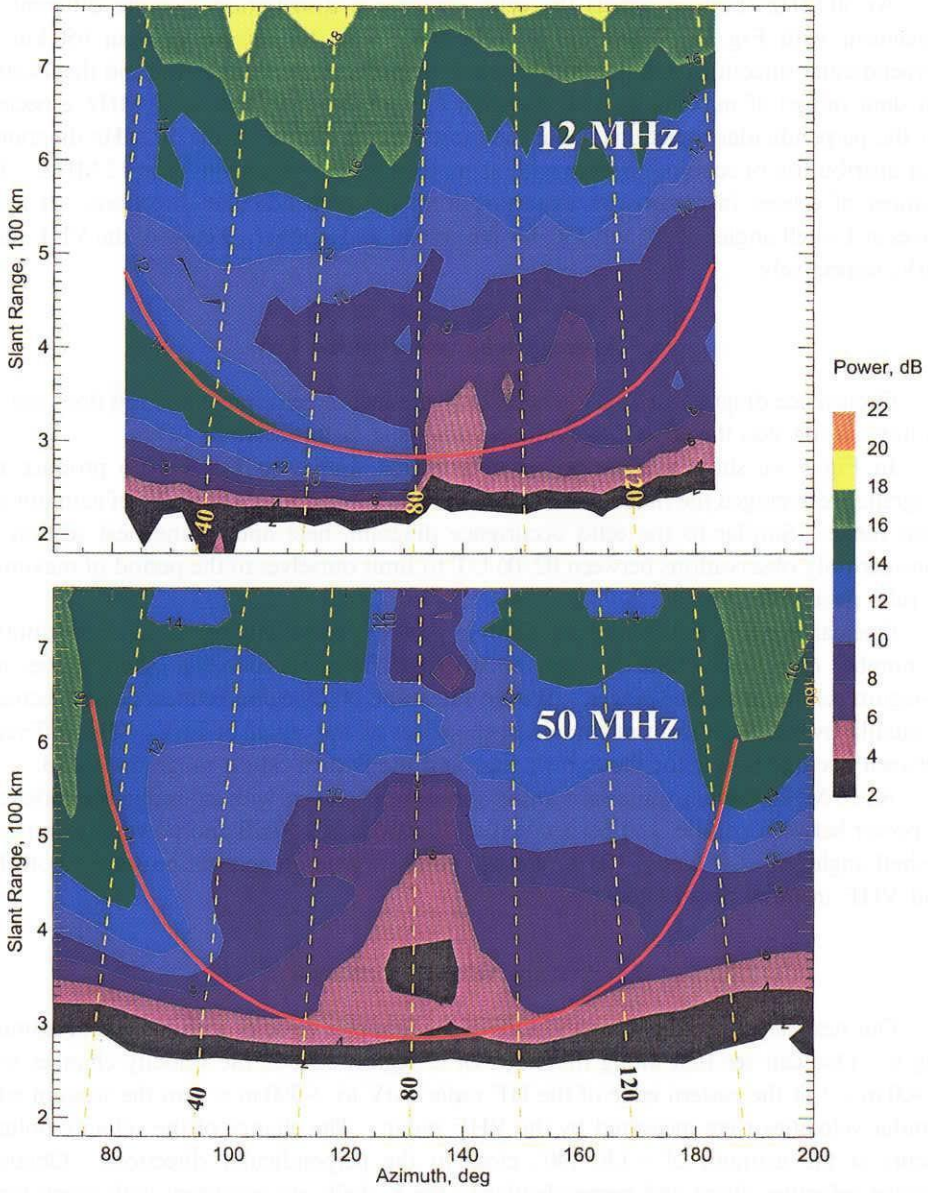

Fig. 5. The same as Fig. 4, but for the average power.

8. 12- and 50-MHz velocities: Point-by-point comparison

From the velocity comparison at HF and VHF (the previous section) one can conclude that average HF and VHF velocities are comparable, to a first approximation. Such a conclusion, however, needs to be refined since, as it is well known on the basis of VHF measurements, different types of ionospheric echoes have different mean Doppler

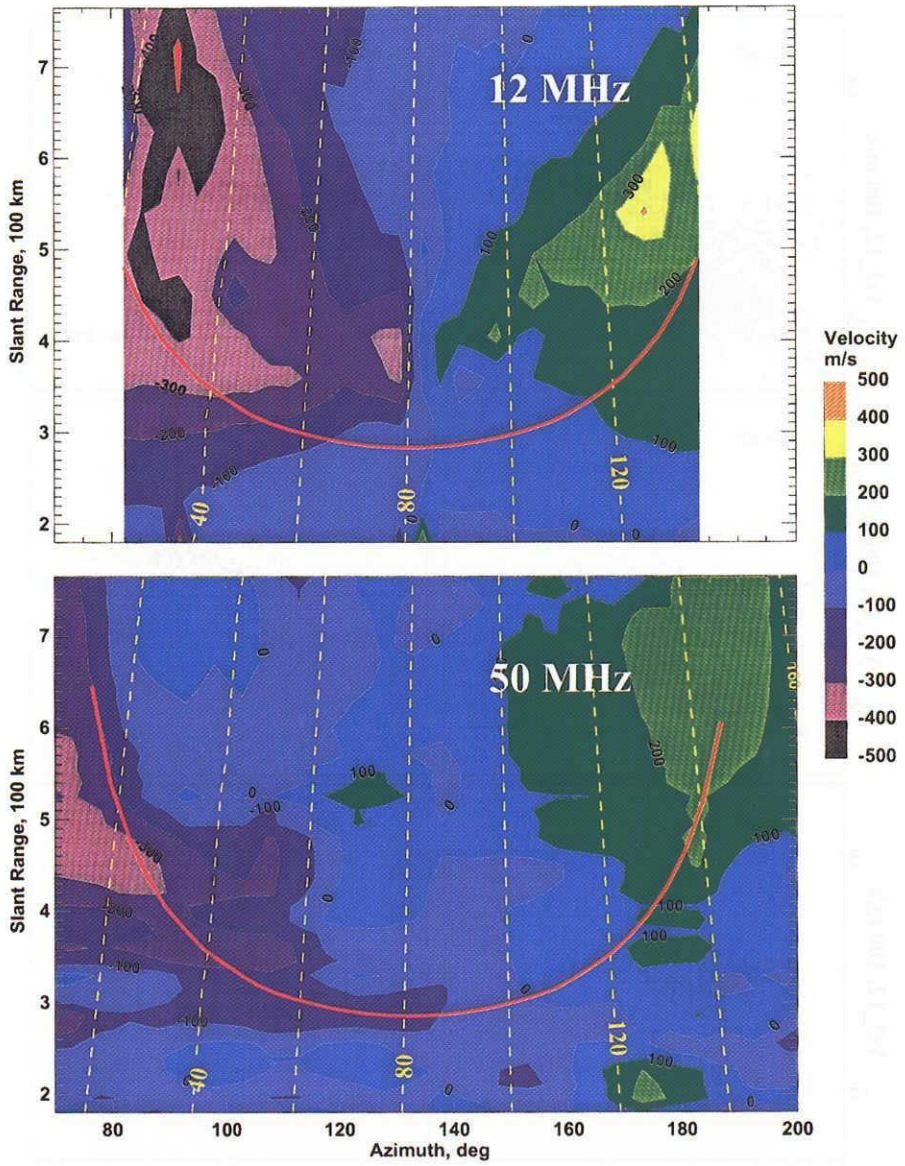

Fig. 6. The same as Fig. 4, but for the average Doppler velocity.

shifts and the variation of Doppler velocity with the L-shell (flow) angle also depends strongly on echo type (Fejer and Kelley, 1980; Haldoupis, 1989). Moreover, Makarevitch *et al.* (2001) showed that the HF echoes with high- and low-velocities should be considered separately.

In this section we produce a scatter plot of HF velocities versus VHF velocities for 6 azimuths of observations, over a period of 00–24 UT for all 23 days of observations, and consider so called "nearly simultaneous" points, Fig. 7. By definition, some measurement

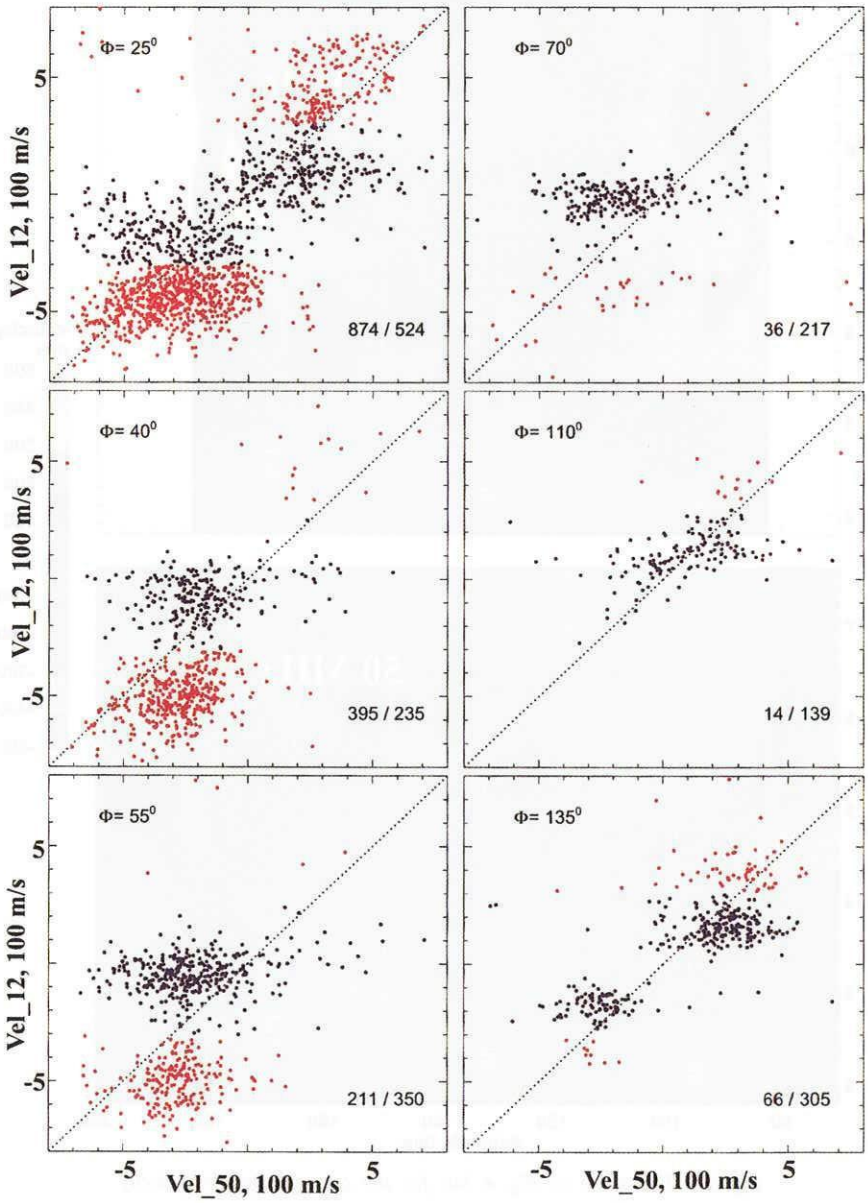

Fig. 7. Velocity of 12-MHz echoes versus velocity of 50-MHz echoes for 6 azimuths. Average value for the L-shell angle ϕ is shown in the top left corner of each panel. For each azimuth, nearly simultaneous measurements at all distances are considered. Red (blue) dots correspond to those echoes whose velocity magnitudes were larger (smaller) than the critical velocity of 320 ms^{-1}. Number of red dots / number of blue dots is shown in the right bottom corner of each panel.

at 12 MHz for the azimuth az_{12}, slant range r_{12}, and time t_{12} was considered to be "nearly simultaneous" with a measurement at 50 MHz at az_{50}, r_{50}, t_{50} if $|az_{12}-az_{50}|<5^{\circ}$, $|r_{12}-r_{50}|<15$ km, and $|t_{12}-t_{50}|<60$ s. In total, 552 hours of observations were considered (*versus* 35 hours in Makarevitch *et al.*, 2001).

We indicated in the top left corner of each panel of Fig. 7 the mean L-shell angle ϕ for each specific radar direction. Angle ϕ progressively increases as one moves from the easternmost Syowa East beam 15 ($\phi\cong 25^{\circ}$) to the westernmost Syowa South beam 0 ($\phi\cong 135^{\circ}$). The other 4 beams considered are Syowa East beams 10, 7, 2, and Syowa South beam 6.

One can clearly see the existence of two echo populations: high- and low-velocity points. We divided all echoes according to the magnitude of 12-MHz Doppler velocity: red (blue) dots are echoes with $V>V_{crit}$ ($V<V_{crit}$), $V_{crit}=320$ m s^{-1}. The number of red/blue points is shown in the right bottom corner of each panel. The difference (vertical distance) between two clouds of points appears to be increasing with ϕ for the first four panels. No difference between negative and positive velocities (morning and evening sectors of observations for the first 4 panels, respectively) can be noticed. Two echo types are well seen for both negative and positive HF velocities. There is a drastic difference between variations of number of high- and low-velocity points with angle ϕ increase. If low-velocity echoes occur at all directions, the high-velocity echoes are rare at the perpendicular directions (the smallest numbers for high-velocity echoes of 36 and 14 are at $\phi=70^{\circ}$ and 110°).

The ratio of 12- to 50-MHz velocity magnitudes depends strongly on whether one deals with low- or high-velocity 12-MHz echoes. For the blue dots the velocity magnitude at 50 MHz is almost always larger than that at 12 MHz ($V^{50}\gg V^{12}_{low}$, where index "low" indicates low-velocity 12-MHz echoes). For the red dots the situation seems to be the opposite ($V^{50}<V^{12}_{high}$, red cloud for negative (positive) velocities is shifted to the right (left) from the dotted line of ideal coincidence, index "high" indicates high-velocity 12-MHz echoes).

9. Doppler velocity *versus* L-shell angle

In this section we study high- and low-velocity echoes using a different approach, namely we make scatter plots of HF and VHF velocities versus L-shell angle. Thus for each radar cell (slant range-azimuth) we consider all available data points rather than present one averaged value as in Fig. 6.

Figure 8 shows a scatter plot of velocity versus L-shell angle for 30-min event on March 17, 1997, 0100-0130 UT. This event was studied by Koustov *et al.* (2001), who considered the variation of the average power and velocity with range. Panel (a) represents data for HF measurements and panel (c) shows data for VHF measurements. The scale for the L-shell angle is given at the bottom of panel (e). For each echo the aspect angle was calculated by assuming one generic electron density profile as explained in Section 5, and we indicate the magnitude of the aspect angle by the color of the point. Color scheme is given in panel (a). Panels (b) and (d) show the histograms of velocity distribution for 12 and 50 MHz, respectively. Total number of points is indicated in the bottom right corner of panels (b) and (d). The scale for panels (b) and (d) is given at the

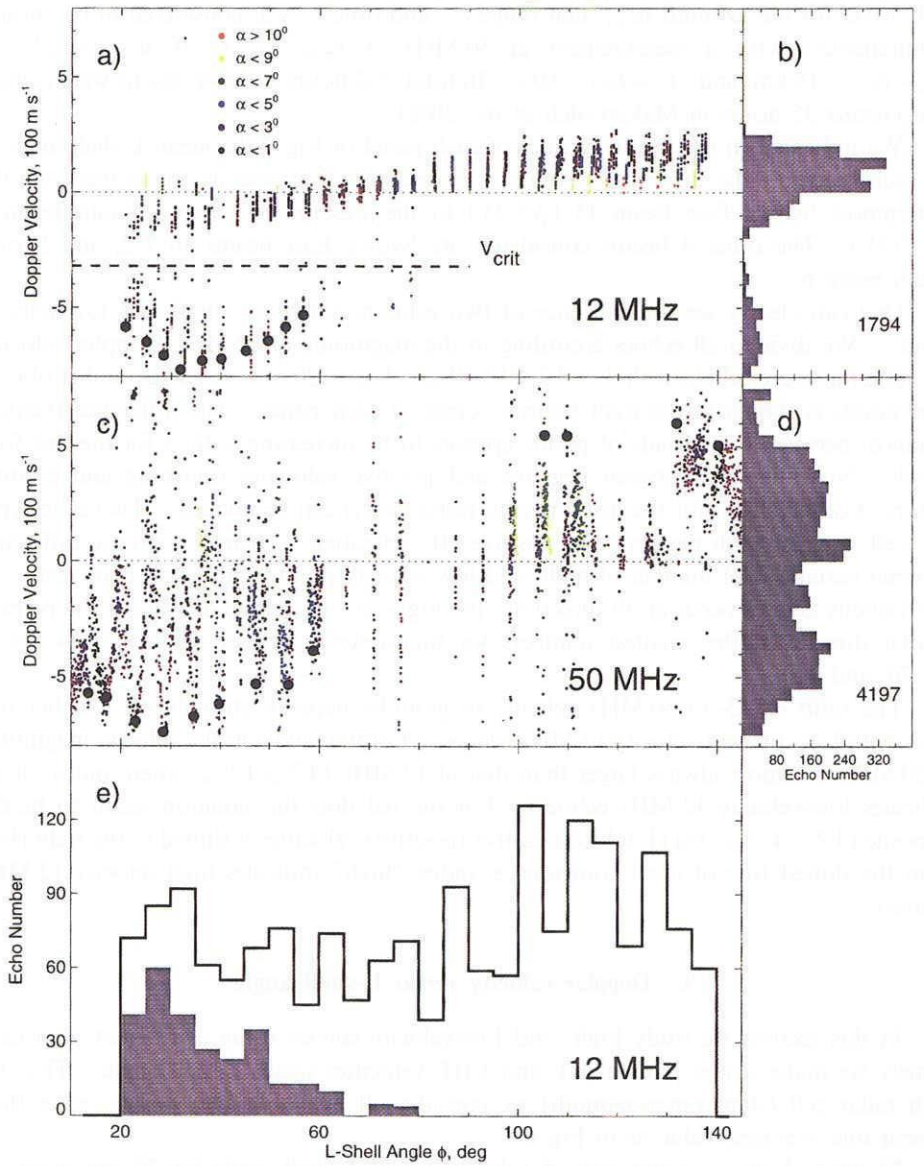

Fig. 8. Doppler velocity versus L-shell angle at (a) 12 and (c) 50 MHz for March 17, 1997, 0100–0130 UT. The aspect angle for each point is color coded as indicated in panel (a). The horizontal dashed line in (a) corresponds to the critical velocity of $-320\ ms^{-1}$. The large black dots are maxima of averaged velocity along some radar beams as described in the text. Right panels are histograms of velocity distribution for (b) 12- and (d) 50-MHz radars. Total number of echoes at each frequency is indicated in the bottom right corner of panels (b) and (d). Panel (e) is the histogram of number of echoes (in 5°-wide bins) versus the L-shell angle at 12 MHz. Solid line corresponds to the total number of echoes and the shaded area corresponds to the number of those echoes whose velocity magnitude was larger than the critical value (points below the dashed line in (a)). The scales for panels (a), (c), and (e) are shown at the bottom of panel (e) and the scales for panels (b) and (d) are shown at the bottom of panel (d).

bottom of panel (d).

The most prominent feature in (a) is the existence of two populations of echoes, high- and low-velocity 12-MHz echoes. The low-velocity echoes have relatively small Doppler velocity magnitudes (<200 m s^{-1}) and they present at all L-shell angles ϕ. High-velocity points have relatively large velocity magnitudes ($>\sim300$ m s^{-1}) and they exist only for $\phi<\sim60°$. The presence of two echo types is obvious not only from the panel (a), but also from the histogram (b), where two maxima can be seen, one at ~500 m s^{-1} and another one at ~0 m s^{-1}.

We believe that these two populations or species correspond to 2 different mechanisms of echo formation, and for this reason we consider data separately for echoes with velocity magnitudes larger and smaller than $V_{crit}=320$ m s^{-1}. We indicate the value of V_{crit} by dashed line in panel (a). In addition to just described separation according to the velocity magnitude, velocities of two echo species seem to have different variations of the Doppler velocity with the L-shell angle. The high-velocity echoes exhibit first increase of the velocity magnitude with ϕ for $20°<\phi<35°$ and then decrease for $35°<\phi<60°$. The Doppler velocity of the low-velocity 12-MHz echoes, on the other hand, increases with ϕ for all directions exhibiting a "cosine-like" variation.

If one concentrates on the 50-MHz part of the diagram, panels (c) and (d), no distinct echo populations can be identified. The histogram (d) shows rather homogeneous distribution: one can find any specific velocity magnitude with approximately equal probability, except for the very large velocities $V>600$ m s^{-1}. There are some kind of V-structures both for small ($\phi<60°$) and large ($\phi>120°$) L-shell angles. For $\phi<60°$, echoes with small aspect angles (black and dark blue dots) tend to have large velocity magnitudes; they are generally located at the bottom of V-structures.

The V-like structures in Fig. 8 are in no doubt associated with the velocity attenuation with the aspect angle known for VHF echoes (Ogawa *et al.*, 1982; Nielsen, 1986; Kustov *et al.*, 1994). Each V-structure is in fact the data from one of the radar beams. As the range and L-shell angle changes along the beam, so does the aspect angle, reaching at some point perfect condition ($\alpha=0$). Since phase velocity of plasma waves is expected to have maximum at a perfect aspect angle, V-structures in Fig. 8 are simply a different form of representation of the velocity variation with the aspect angle. V-structures for $\phi\sim90°$ are not well seen because here the L-shell angle does not change much as one goes along individual radar beams. One can conclude that all "VHF low-velocity points" in (c) are actually echoes with poor aspect angles. Thus Fig. 8 indicates that there is no special "low-velocity" kind of echoes at VHF.

One must bear in mind that values of the aspect angle in Fig. 8 are calculated from the density distribution model. The actual aspect angle conditions might be different from the ones given by the model. For this reason, not all black points are at the bottom of V-structures. Having this in mind, only maximum velocities should be considered for the comparison at HF and VHF since others are significantly affected by the aspect angle attenuation.

Because there is a substantial data spread for each radar cell, to obtain statistically meaningful estimate of the maximum velocity, we performed one more type of analysis. For each radar beam, we considered all points with Doppler velocity magnitudes larger than critical value V_{crit} (for 12 MHz, points below the dashed line in (a)). We found the

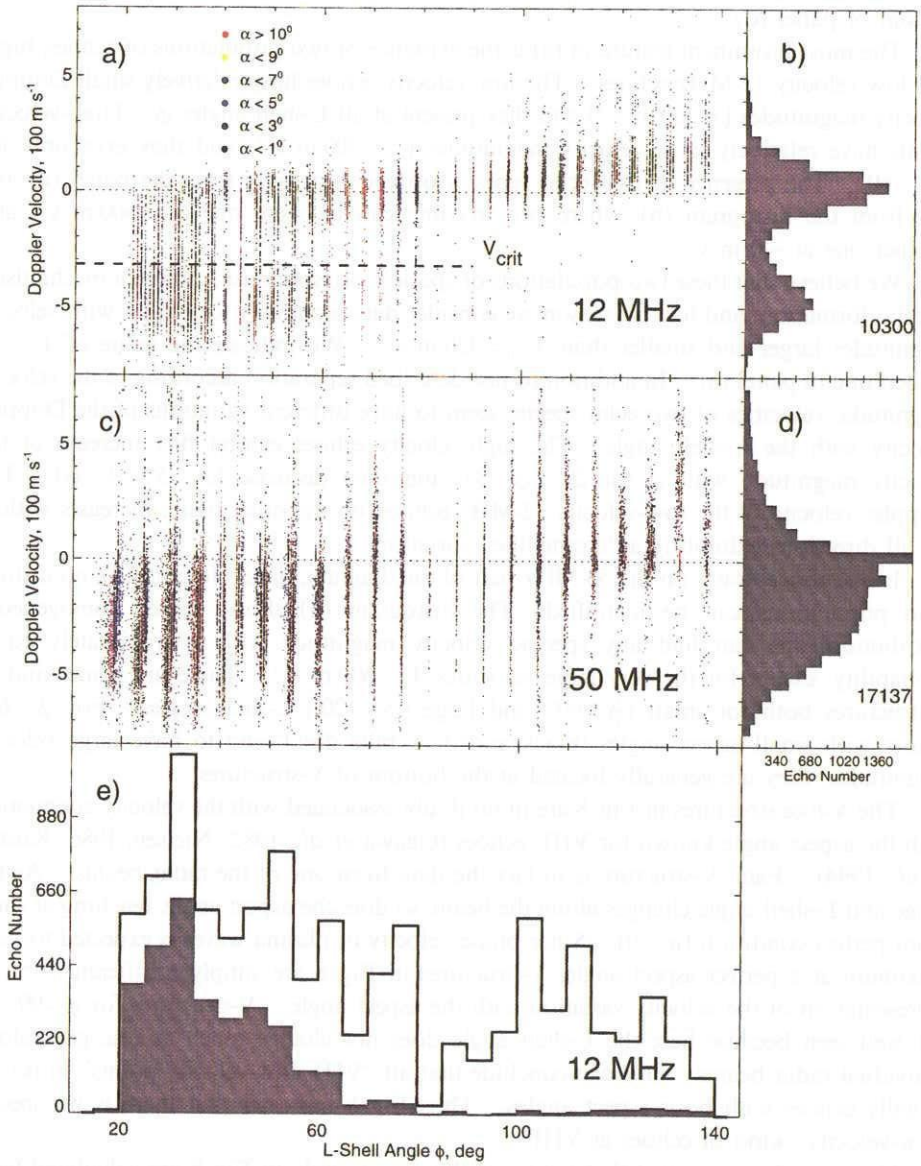

Fig. 9. The same as Fig. 8, but for 23 days in March 1997, 0200–0600 UT, nearly simultaneous points (see description in the text).

average of these points for each slant range (thus we obtained one point for each vertical line in (a) and (c)) so that the maximum average velocity of high-velocity echoes in each radar beam was calculated. The obtained velocities are plotted in panels (a) and (c) by large black dots. These points should correspond to zero aspect angle measurements since velocity magnitude maximizes at perfect aspect angle.

Now we can compare directly L-shell dependencies for high-velocity echoes at 12 and 50 MHz, large black dots in panels (a) and (c). One can see that, overall, the two trends

are similar. The only distinguishable by eye difference between two curves is that 12-MHz curve appears to be shifted with respect to that at 50 MHz. The latter maximizes at $\phi \cong 30°$ and the former at $\phi \cong 35°$. Because of this shift, the velocity magnitudes at HF are slightly larger (smaller) than that at VHF for $\phi > 30°$ ($\phi < 30°$) if one compares velocities for the same value of ϕ (drawing vertical line through (a) and (c)). If one compares 50-MHz echoes with low-velocity 12-MHz echoes, it is evident that velocity magnitude at 50 MHz is always larger than that at 12 MHz. Thus symbolically we can write for magnitudes $V^{50} \gg V^{12}_{\text{low}}$ for all ϕ, $V^{50} > V^{12}_{\text{high}}$ for $\phi < 30°$, and $V^{50} < V^{12}_{\text{high}}$ for $\phi > 30°$.

Finally, in the panel (e) we present the histogram of number of 12-MHz echoes at various L-shell angles ϕ. We indicated the total number of echoes for 5°-wide L-shell angle bins by the solid line and the number of high-velocity echoes (with velocity magnitudes larger than V_{crit}) by the shaded area. The difference or the vertical distance between solid curve and shaded area thus represents the number of low-velocity echoes. Total number of points for this particular event is approximately the same for all directions of the FoV. The number of high-velocity points decreases steadily from $\phi = 20°$ to $\phi = 90°$. For $\phi > 90°$ there are no high-velocity echoes. Notice also that the number of low-velocity points (the vertical difference) slightly increases with ϕ.

In Fig. 9 we present data for the expanded period of 23 days (02–06 UT). Here we used only "nearly simultaneous" measurements (as defined in the previous section) to have diagram readable. One can notice that in Fig. 9 the relative number of points with poor calculated aspect angles is lower than in Fig. 8 and that two peaks in the distribution of velocities, corresponding to two species of 12-MHz echoes, are more distinct. The distribution of the 50-MHz velocities also becomes "smoother", with maximum at ~ 0 ms^{-1}. The fact that VHF radar sees some echoes with low velocities is entirely due to the poor aspect angle conditions for these echoes. The peaks in Fig. 8 are less prominent (two at 12 MHz and one at 50 MHz) than in Fig. 9 because of the larger relative number of echoes with poor aspect angles. In Fig. 9e one can also observe that the number of high-velocity echoes decreases with ϕ, number of low-velocity echoes is almost the same for all ϕ, except for some difference in eastern and southern sectors.

10. Power and width versus L-shell angle

Since HF echoes can be of two types, we decided to look more carefully at the L-shell variation for the echo power of each type, and, in addition, we study whether there is any difference between spectral widths of these two HF echo types.

Figure 10 shows the L-shell angle variation of the spectral (a) power and (b) width. We used here again small 30-min database for all, not joint points. As in Fig. 7 we labelled each point according to its magnitude of Doppler velocity: red (blue) dots are echoes with velocity magnitude larger (smaller) than V_{crit}. Large red dots and blue crosses in Fig. 10 are averaged values of the spectral power and width calculated using 5°-wide L-shell angle bins for high- and low-velocity HF echoes, respectively. Also in Fig. 10 we show standard deviations and numbers of points used for averaging for each bin and each type of echoes. The average value was not plotted if the number of points in a bin was too small. Direction corresponding to the boundary between two HF radars is at $\phi \cong 80°$ and we connected the average values for each radar separately.

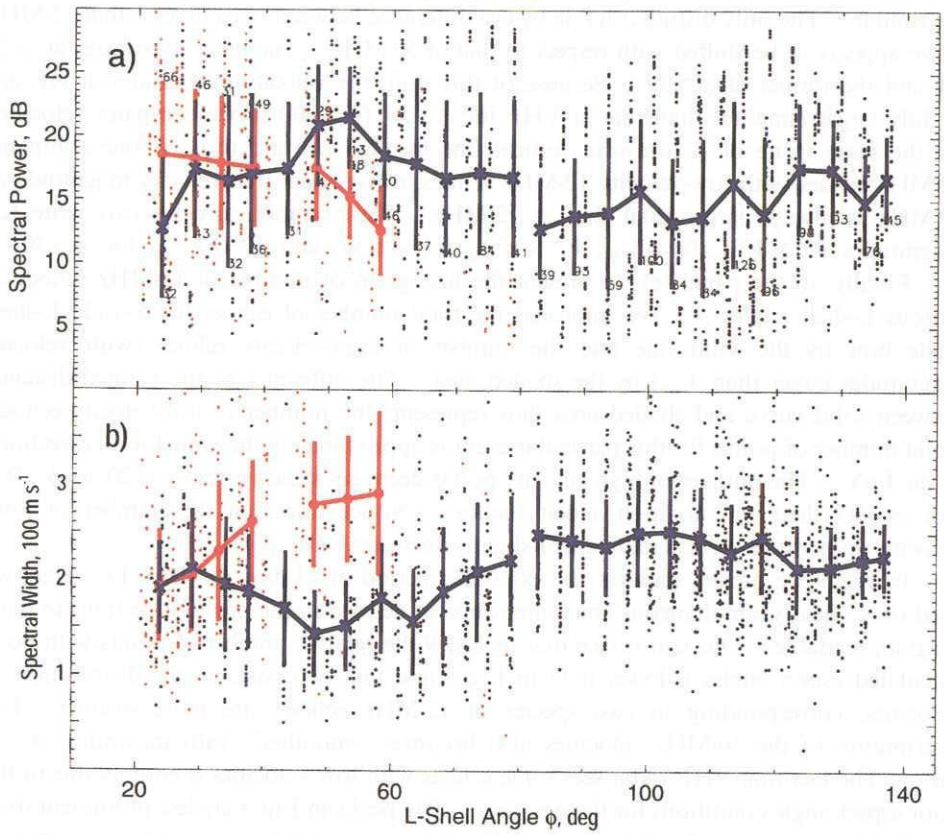

Fig. 10. Spectral power at HF versus L-shell angle for 0100–0130 UT on March 17, 1997, panel (a). Red (blue) points are echoes with velocity magnitude larger (smaller) than $V_{crit}=320$ ms^{-1}. Averaged (for 5°-wide bins in L-shell angle) values, standard deviations and numbers of points are indicated for high- and low-velocity HF echoes. The spectral width at HF versus L-shell angle is shown in panel (b).

One can notice from Fig. 10 that high-velocity echoes (red dots) tend to have larger power than low-velocity echoes and that there is a tendency for the power to decrease with L-shell angle. The power of low-velocity echoes is approximately the same for all ϕ, albeit the spread is significant here.

The high-velocity echoes have the same or somewhat smaller widths as the low-velocity echoes for $\phi<\sim30°$. For $30°<\phi<60°$, the high-velocity echoes have larger widths. This change occurs because of a general increase in the width of HF high-velocity echoes with ϕ. Width of the low-velocity echoes is slightly increased at perpendicular directions, $\phi\sim90°$.

In Fig. 11 we present results for the entire database of joint points (23 days for 02–06 UT). These diagrams generally support our conclusions drawn from the 30-min interval. One can see here more clearly that the power of HF high-velocity echoes is stronger than the power of low-velocity echoes, and that the Syowa East echoes are typically stronger than Syowa South ones, in agreement with the data presented in Fig. 5. We can state that

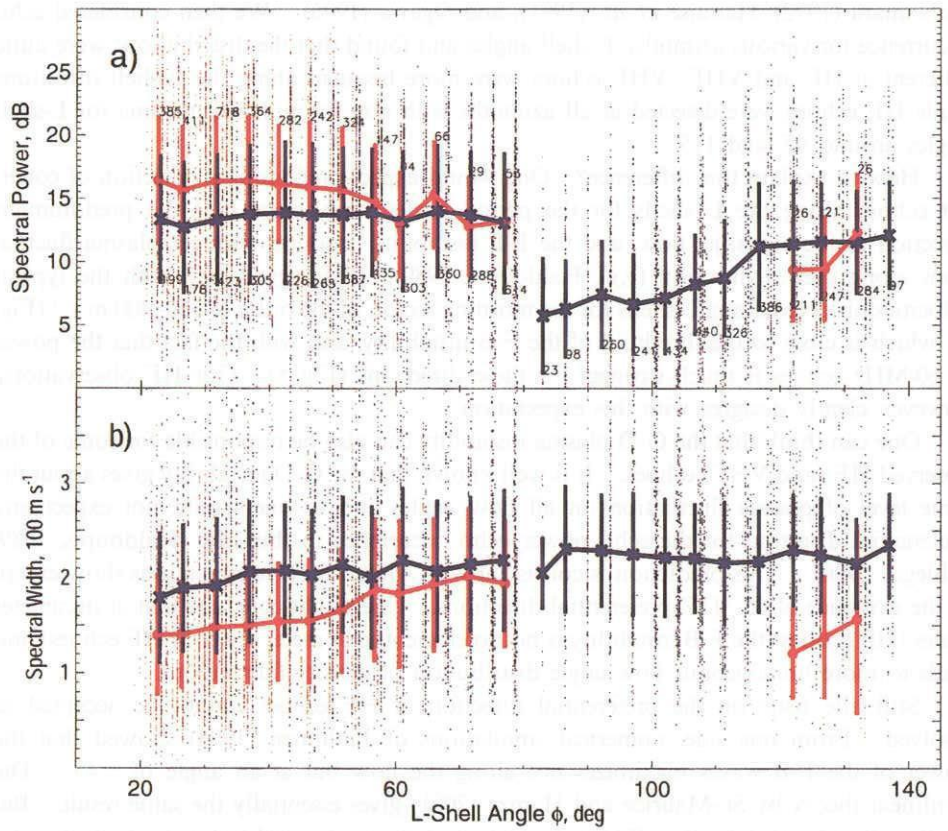

Fig. 11. The same as Fig. 10, but for 23 days of nearly simultaneous measurements in March 1997, 0200–0600 UT.

a quasi-homogeneous power-azimuth distribution of HF echoes discussed by Koustov *et al.* (2001) is rather an exception (the difference in power and echo occurrence between eastern an southern sectors of observations will be discussed later in the next section). We also can more clearly see that high-velocity HF echoes have smaller width than low-velocity echoes and the width of low-velocity echoes is about the same at all L-shell angles.

11. Discussion

In this paper we presented statistics for several characteristics of HF and VHF auroral echoes observed from the same location at Syowa, Antarctica. 23 days of two-frequency measurements in March of 1997 were considered. Our main goal was to explore variations of echo characteristics with the azimuth/L-shell angle of observations. More detailed analysis was performed for the morning sector (westward electrojet), between 02 and 06 MLT, where we had about 92 hours of measurements.

We demonstrated that both HF and VHF auroral echoes at short ranges of $r<800$ km occur more frequently during the nighttime, in agreement with previous studies, *e.g.*

McNamara (1972), Hanuise *et al.* (1991), and Ogawa (1996). We then considered echo occurrence for various azimuths/L-shell angles and found that the distributions were quite different at HF and VHF; VHF echoes were more frequent along the L-shell directions while HF echoes were detected at all azimuths with non pronounced maxima for L-shell angles around 45° and 115°.

How to explain this difference? One would expect predominant detection of coherent echoes along the L shells for the period under study since it is the predominant direction of the electrojet flow, and the F-B instability produces stronger plasma fluctuations along such a direction (*e.g.*, Haldoupis, 1989). This agrees well with the typical velocities observed along L shells for the morning sector, of the order of 350–400 m s^{-1} (Fig. 6), which is close to the threshold of the F-B instability, and with the fact that the power of 50-MHz echoes is much stronger for these directions (Fig. 5). Our HF observations, however, clearly disagree with this expectation.

One can think that the G-D plasma instability can also be responsible for some of the observed HF (and VHF) echoes. It is well known that the G-D instability gives about the same level of plasma fluctuations at all flow angles and so one would not expect any preferential direction for the echo power/echo occurrence in this case (Haldoupis, 1989; Schlegel, 1996). This prediction is consistent with what our HF observations show except of the existence of 45°/115° preferential directions. One might conclude that at decameter scales (HF echoes) the F-B instability is not so efficient as at meter scales (VHF echoes) and leads to more homogenous flow angle distribution of density fluctuations.

Still, the issue on the preferential direction of HF echoes cannot be accepted as resolved. From one side, numerical simulations of Janhunen (1994) showed that the power of the F-B waves maximizes not along the flow but at an angle of ~45°. The nonlinear theory by St.-Maurice and Hamza (2001) gives essentially the same result. But on the other hand, why the effect is important at decameter and not important at meter scales is still unclear.

One can also think about possibility of difference in average heights of HF and VHF echoes as discussed by Koustov *et al.* (2001) and Makarevitch *et al.* (2001). In this case, since both the F-B and G-D instabilities are easier to excite along the vector of the relative electron-ion drift, one might have slightly different preferential directions for the instabilities to occur at various heights. One may have up to ~10° azimuthal difference in this case. This is not enough to explain the observed ~25° deviation of the HF echo occurrence maxima from the direction along the flow. In addition, such explanation can be accepted for the Syowa East morning observations but not for the Syowa South observations, for which the direction of current rotation is opposite to the required one.

In our opinion, the preferential detection of HF echoes at ~45°/115° directions indicates that the processes of VHF and HF echo formation might be not exactly the same. The fact that the power of HF echoes did not show any specific maximum at L-shell angles of 45° tells us that the additional sources of HF echoes, if they exist, provide about the same power of echoes as the traditional F-B and G-D instabilities and identification of these additional sources is not possible by looking just at the power of coherent echoes.

In the past, Dimant and Sudan (1997) developed the theory of the thermo-diffusion instability at the electrojet bottom side. This instability is more easily excited at an angle of ~45° with respect to the flow. Thus it could effectively provide a shift of the echo

occurrence maximum both at VHF and HF. However, since this instability is more efficient at decameter scales, the effect can only be seen in the occurrence of HF echoes. Other potential sources of irregularities at 90–100 km heights are the neutral wind and neutral turbulence (Kagan and Kelley, 1998, 2000; Gurevitch *et al.*, 1997; Ogawa *et al.*, 2001). Irregularities produced through these processes are controlled by neutral wind that might provide some preferential direction for the echo detection though the question requires further consideration.

The performed in this study velocity comparison supports our major hypothesis that HF coherent echoes might have additional sources. We showed, similar to Makarevitch *et al.* (2001), that there are two distinct populations of 12-MHz echoes, the high- and low-velocity echoes. New finding of the present study is that these echo populations exhibit completely different dependencies of their Doppler velocity upon the L-shell angle.

We found that low-velocity 12-MHz echoes exist for all radar directions. Their Doppler velocity variation with the L-shell angle, Figs. 8 and 9, can be roughly described by the cosine law if one assumes the maximum velocity of the order of 100–150 m s^{-1}. This would suggest that the G-D instability or secondary F-B waves are responsible for these echoes. However, velocities of these echoes is significantly, up to a factor of 2, smaller than the velocities of simultaneously observed VHF echoes. Not less important is the fact of fairly fixed values of low-velocity population maxima, 100–150 m s^{-1}. These values are suspiciously close to the neutral wind velocities observed at auroral latitudes, *e.g.* Tsunoda (1988). And finally we failed to reveal an isolated low-velocity echo population in 50-MHz data, Figs. 8 and 9. Here VHF low-velocity echoes seem to be an integral part of the scatter plot.

We have little doubt about the nature of the high-velocity VHF and HF echoes. These are related to the Farley-Buneman plasma instability. Such echoes were observed mostly along the L shells. Their power was generally larger than that of low-velocity echoes, and it was decreasing with the L-shell angle. We also demonstrated using larger data set, Fig. 11, that the high-velocity echoes were more narrow.

One important result concerning these echoes is the velocity change with the L-shell angle, Figs. 8 and 9. The effect is well seen at both HF and VHF. It was thought for a long time that type 1 echoes observed at small flow angles, inside the F-B instability cone, do not exhibit any velocity variation with flow angle (*e.g.*, Nielsen and Schlegel, 1983). Recently Nielsen *et al.* (2002) showed that the phase velocity for VHF radar frequency of 140 MHz is maximized at zero flow angle and slowly decreases up to flow angle of 40° where it is equal to the ion acoustic speed. Similar feature at HF was discussed recently by Uspensky *et al.* (2001). In another study by Milan and Lester (2001) it was shown that some HF echoes (type 3 and 4 in their notation) exhibit quite peculiar dependence of the Doppler velocity upon the L-shell angle. Velocity magnitudes of such echoes maximized neither along nor perpendicular to the flow at L-shell angles of 25–35°. We found, Fig. 8, that both VHF and HF velocity magnitudes are largest at the L-shell angles of ~30°, and, in this sense, our results support strongly the result of Milan and Lester (2001). We think, however, that the velocity maximum shift from L-shell angle of 0° is most likely due to some departure of the flow from the L-shell direction, rather than due to some plasma-physical mechanism. Indeed, in the morning sector and at auroral latitudes one might expect additional "curving" of the flow towards the magnetic pole for the two-cell

convection pattern. If the amount of flow curving for the eastern part of FoV was of the order of 30° then our results are in good agreement with the results of Nielsen *et al.* (2002). One can ask why the low-velocity HF echoes do not show larger velocities for the L-shell angle about 30°. In our opinion, the reason is that these echoes are originated not only from the F-B and G-D instabilities but also from other instabilities that are not so much controlled by the ionospheric electric field.

The rotation of the flow from the direction of magnetic L shells could also be the reason for very small number of the high-velocity HF echoes for the Syowa South radar. Indeed, in a case of exactly L-shell aligned flow, the distributions in Figs. 8 and 9 would be symmetric with respect to the direction $\phi = 90°$; both HF radars would detect almost the same number of the high-velocity echoes. The current rotation (electric field rotation) of the order of 30° would shift this direction towards larger L-shell angles ($\phi \cong 120°$) and would shift the F-B instability cone orientation for the Syowa South radar ($\phi \cong 150°$). In this situation, the detection of high-velocity echoes here would be possible only at azimuths larger than 183°, beyond the Syowa South FoV. In the consideration above we assumed that electric field magnitudes are about the same in the Syowa South and Syowa East FoVs. Thus it is not the L-shell angle that controls the generation of the high-velocity HF echoes, but rather the electrojet/electric field direction (and certainly its magnitude).

Statistically, the power measured by the Syowa East radar was larger than the power measured by Syowa South, Fig. 5, by 6–8 dB. This difference between the power of two radars is also obvious in Fig. 11a and for echo occurrence in Fig. 4 where the number of echoes is significantly lower for the Syowa South radar. This fact, unnoticeable on the basis of the 30-min observational period alone (Plate 1c of Koustov *et al.* (2001) and our Fig. 10a), is most likely due to the fact that the Syowa South radar operated under different technical and observational conditions. It was discovered that the Syowa South radar had higher noise level in the receiver system. Also, to avoid interference with the Syowa East radar (FoVs of both radars slightly overlap) the base sounding frequency for Syowa South was chosen to be ~11 MHz versus ~12 MHz for the Syowa East. The difference between radar frequencies could result in different amount of ray bending and hence to slightly different altitudes of scatter (Koustov *et al.*, 2001; Makarevitch *et al.*, 2001). For these reasons, all conclusions of the present study were drawn on the basis of observations from the Syowa East radar and we used Syowa South data only as a reference.

Finally, we have to note that no special attention has been paid in this study to meteor echoes. It is accepted that their contribution to echo detection at Syowa is not negligible (*e.g.*, Ogawa *et al.*, 1985, 2001). In the previous studies by Fukumoto *et al.* (1999, 2000), Makarevitch *et al.* (2001) and Ogawa *et al.* (2001) attempts have been made to exclude meteor echoes from the data base. Such approach is certainly successful in eliminating isolated in time and space reflections (that are more likely to be truly meteor reflections) but not reflections occurring simultaneously with the auroral ionospheric scatter. Contrary to this approach, in the present study we considered all available echoes at short ranges. We expect, consequently, that some of the low-velocity VHF and especially HF echoes were, in fact, meteor scatter.

Hall *et al.* (1997) reported on correlation of HF Doppler velocities of short range echoes and neutral winds measured independently by a MF radar. These authors assumed that all detected echoes were meteor scatter. We believe that in our observations there was

a mixture of ionospheric and meteor echoes with predominance of ionospheric echoes. This is supported by several facts. Syowa echoes were more frequent at 1-2 UT and not in the late morning hours and, when occurred, they typically had quite an extensive spatial and temporal coverage. We also analyzed HF/VHF data in the evening sector and found results similar to the ones presented in the present paper for the morning sector. Additional support comes from the revealed features of echo characteristics, for example, velocities were quite often large, >100 m s^{-1}, more than typical meteor echo velocities, and the HF spectra were quite broad. We do believe, however, that low-velocity echoes were strongly affected by neutral particle motions, and in this sense our results are in agreement with Hall *et al.* (1997).

12. Conclusions

In this study a statistical comparison between echo characteristics at two significantly different radar frequencies (12 and 50 MHz) has been performed. We considered one month of nearly simultaneous two-frequency measurements in a broad range of flow and aspect angles. We concentrated on the azimuth/L-shell variation of such echo parameters as echo occurrence, spectral power, mean Doppler shift and spectral width.

We showed that overall echo occurrence within the radars' common FoV varied with the time of the day in a similar manner at both radar frequencies and had maxima at post-midnight hours. However, when specific radar directions were compared, it was found that the echo occurrence depended on the azimuth/L-shell angle of measurements. We explored the nature of this difference using two approaches.

First, we considered data for the morning sector, for which the echo occurrence was the highest, and found that while VHF echoes were more frequently detected along the L shells, HF echoes were observed at all L-shell angles with some broad maximum at angles around 45° and 115°. Azimuthal distribution of the power was found to have a strong maximum along L shells at VHF and to be more or less homogeneous at HF.

We then turned our attention to the velocities of echoes at various L-shell angles. We showed that HF echoes can be divided into two populations, the high- and low-velocity echoes, while VHF echoes are of only one kind, the high-velocity echoes and their aspect-attenuated counterparts. We also explored the behavior of the HF power and spectral width with L-shell angle for these two echo populations and showed that the high-velocity echoes are stronger and more narrow that the low-velocity ones.

We related the high-velocity VHF and HF echoes to the F-B plasma instability. The low-velocity HF echoes were associated with several possible sources. We argued that these echoes are originated not only from scatter on secondary F-B and G-D waves but also on irregularities associated with other plasma processes in the auroral E region. We assumed that the thermo-diffusion instability at the bottom of the electrojet layer or instabilities originated from the neutral wind contribute significantly to the formation of the decameter scale irregularities (HF echoes).

Acknowledgments

A.V.K. acknowledges the Solar-Terrestrial Environment Laboratory of the Nagoya

University for funding during his stay in Japan. The work was also supported by an NSERC grant (Canada) to A.V.K. The authors thank M. Lester, J.-P. St.-Maurice and D. Danskin for discussions of the results and C. Haldoupis for criticism.

The editor thanks Dr. R. Fujii and another referee for their help in evaluating this paper.

References

Baker, K.B. and Wing, S. (1989): A new magnetic coordinate system for conjugate studies at high latitudes. J. Geophys. Res., **94**, 9139–9143.

Bilitza, D. (1997): International Reference Ionosphere -Status 1995/96. Adv. Space Res., **20**, 1751–1754.

Dimant, Ya.S. and Sudan, R.N. (1997): Physical nature of a new cross-field current-driven instability in the lower ionosphere. J. Geophys. Res., **102**, 2551–2563.

Fejer, B.G. and Kelley, M.C. (1980): Ionospheric irregularities. Rev. Geophys., **18**, 401–454.

Fukumoto, M., Nishitani, N., Ogawa, T., Sato, N., Yamagishi, H. and Yukimatu, A.S. (1999): Statistical analysis of echo power, Doppler velocity and spectral width obtained with the Syowa South HF radar. Adv. Polar Upper Atmos. Res., **13**, 37–47.

Fukumoto, M., Nishitani, N., Ogawa, T., Sato, N., Yamagishi, H. and Yukimatu, A.S. (2000): Statistical study of Doppler velocity and echo power around 75 deg magnetic latitude using data obtained with the Syowa East HF radar in 1997. Adv. Polar Upper Atmos. Res., **14**, 93–102.

Greenwald, R.A. *et al.* (1995): DARN/SuperDARN: A global view of the dynamics of high-latitude convection. Space Sci. Rev., **71**, 763–796.

Gurevitch, A.V., Borisov, N.D. and Zybin, K.P. (1997): Ionospheric turbulence induced in the lower part of the E region by the turbulence of the neutral atmosphere. J. Geophys. Res., **102**, 379–388.

Haldoupis, C. (1989): A review on radio studies of auroral E region ionospheric irregularities. Ann. Geophys., **7**, 239–258.

Hall, G.E., MacDougall, J.W., Moorcroft, D.R., St.-Maurice, J.-P., Manson, A.H. and Meek, C.E. (1997): Super Dual Auroral Radar Network observations of meteor echoes. J. Geophys. Res., **102**, 14603–14614.

Hanuise, C., Villain, J.-P., Cerisier, J.C., Senior, C., Ruohoniemi, J.M., Greenwald, R.A. and Baker, K. B. (1991): Statistical study of high-latitude E region Doppler spectra obtained with SHERPA HF radar. Ann. Geophys., **9**, 273–285.

Igarashi, K., Ohtaka, K., Kunitake, M., Tanaka, T. and Ogawa, T. (1995): Development of scanning-beam VHF auroral radar system. Proc. NIPR Symp. Upper Atmos. Phys., **8**, 65–69.

Igarashi, K., Ohtaka, K., Kunitake, M. and Kikuchi, T. (1998): Scanning-beam VHF auroral radar at Syowa station. Proc. NIPR Symp. Upper Atmos. Phys., **11**, 154–158.

Janhunen, P. (1994): Perpendicular particle simulation of the *E*-region Farley-Buneman instability. J. Geophys. Res., **99**, 11461–11473.

Jayachandran, P.T., St.-Maurice, J.-P., MacDougall, J.W. and Moorcroft, D.R. (2000): HF detection of slow long-lived *E* region plasma structures. J. Geophys. Res., **105**, 2425–2442.

Kagan, L.M. and Kelley, M.C. (1998): A wind-driven gradient drift mechanism for mid-latitude E-region ionospheric irregularities. Geophys. Res. Lett., **25**, 4141–4144.

Kagan, L.M. and Kelley, M.C. (2000): A thermal mechanism for generation of small-scale irregularities in the ionospheric *E* region. J. Geophys. Res., **105**, 5291–5303.

Koustov, A.V., Igarashi, K., Andrē, D., Ohtaka, K., Sato, N., Yamagishi, H. and Yukimatu, A.S. (2001): Observations of 50- and 12-MHz auroral coherent echoes at the Antarctic Syowa Station. J. Geophys. Res., **106**, 12875–12887.

Kustov, A.V., Uspensky, M.V., Sofko, G.J., Koehler, J.A. and Mu, J. (1994): Aspect angle dependence

of the radar aurora Doppler velocity. J. Geophys. Res., **99**, 2131–2144.
Makarevitch, R.A., Ogawa, T., Igarashi, K., Koustov, A.V., Sato, N., Ohtaka, K., Yamagishi, H. and Yukimatu, A.S. (2001): On the power-velocity relationship for 12- and 50-MHz auroral coherent echoes. J. Geophys. Res., **106**, 15455–15469.
McNamara, A.G. (1972): The occurrence of radio aurora at high latitudes: the IGY period, 1957–1959. Geophysiske Publikasjoner, **29**, 135–149.
Milan, S.E. and Lester, M. (1998): Simultaneous observations at different altitudes of ionospheric backscatter in the eastward electrojet. Ann. Geophys., **16**, 55–68,.
Milan, S. and Lester, M. (1999): Spectral and flow angle characteristics of backscatter from decameter irregularities in the auroral electrojet. Adv. Space Res., **23**, 1773–1776.
Milan, S.E. and Lester, M. (2001): A classification of spectral populations observed in HF radar backscatter from the E region auroral electrojets. Ann. Geophys., **19**, 189–204.
Milan, S.E., Lester, M., Sato, N. and Takizawa, H. (2001): On the altitude dependence of spectral characteristics of decameter-wavelength E region backscatter and the relationship with optical auroral forms. Ann. Geophys., **19**, 205–217.
Nielsen, E. (1986): Aspect angle dependence of mean Doppler velocities of 1-m auroral plasma waves. J. Geophys. Res., **91**, 10173–10177.
Nielsen, E. and Schlegel, K. (1983): A first comparison of STARE and EISCAT electron drift velocity measurements. J. Geophys. Res., **88**, 5745–5750.
Nielsen, E., Del Pozo, C.F. and Williams, P.J.S. (2002): VHF coherent radar signals from the E region ionosphere and the relationship to electron drift velocity and ion acoustic velocity. J. Geophys. Res., **107**, (A1), SIA4-1–SIA4-9, 10.1029/2001JA900111.
Ogawa, T., Balsley, B.B., Ecklund, W.L., Carter, D.A. and Johnston, P.E. (1982): Auroral radar observations at Siple Station, Antarctica. J. Atmos. Terr. Phys., **44**, 529–537.
Ogawa, T. (1996): Radar observations of ionospheric irregularities at Syowa station, Antarctica: A brief overview. Ann. Geophys., **14**, 1454–1461.
Ogawa, T., Igarashi, K., Kuratani, Y., Fujii, R. and Hirasawa, T. (1985): Some initial results of 50 MHz meteor radar observations at Syowa station. Mem. Natl Inst. Polar Res., Spec. Issue, **36**, 254–263.
Ogawa, T., Nishitani, N., Sato, N., Yamagishi, H. and Yukimatu, A.S. (2001): Implications of statistics of near-range Doppler velocity observed with the Syowa East HF radar. Adv. Polar Upper Atmos. Res., **15**, 82–102.
Sahr, J. and Fejer, B.G. (1996): Auroral electrojet plasma irregularity theory and experiment: A critical review of present understanding and future directions. J. Geophys. Res., **101**, 26893–26909.
Schlegel, K. (1996): Coherent backscatter from ionospheric E region plasma irregularities. J. Atmos. Terr. Phys., **58**, 933–941.
St-Maurice, J.-P. and Hamza, A.M. (2001): A new nonlinear approach to the theory of E-region irregularities. J. Geophys. Res., **106**, 1751–1760.
Tsunoda, R.T. (1988): High latitude irregularities: A review and synthesis. Rev. Geophys., **26**, 719–760.
Uspensky, M.V., Koustov, A.V., Eglitis, P., Huuskonen, A., Milan, S.E., Pulkkinen, T. and Pirjola, R. (2001): CUTLASS HF radar observations of high-velocity E-region echoes. Ann. Geophys., **19**, 411–424.
Villain, J.P., Greenwald, R.A., Baker, K.B. and Ruohoniemi, J.M. (1987): HF radar observations of E region plasma irregularities produced by oblique electron streaming. J. Geophys. Res., **92**, 12327–12342.
Villain, J.-P., Hanuise, C., Greenwald, R.A., Baker, K.B. and Ruohoniemi, J.M. (1990): Obliquely propagating ion acoustic waves in the auroral E region: Further evidence of irregularity production by field-aligned electron streaming. J. Geophys. Res., **95**, 7833–7846.

(Received December 20, 2001; Revised manuscript accepted May 8, 2002)